J Appl Electrochem (2009) 39:1633–1642
DOI 10.1007/s10800-009-9849-7

ORIGINAL PAPER

Electrochemical behavior of AZ91D magnesium alloy in phosphate medium: Part II. Induced passivation

Fakiha El-Taib Heakal · Amany Mohammed Fekry · Mohamad Ziad Fatayerji

Received: 25 May 2008 / Accepted: 23 February 2009 / Published online: 13 March 2009

Abstract Induced passivation of AZ91D magnesium alloy in phosphate solution was carried out both chemically, using various inorganic oxidants, namely, molybdate, vanadate and iodate, as well as electrochemically by anodizing the alloy under various controlled overpotentials within the range 0.1–3.4 V. In acidic phosphate (pH 4.5), molybdate and vanadate anions exhibit similar behavior, as they show a dissolution effect at lower concentrations and passivation at higher concentrations. On the other hand, iodate anions shows critical behavior with a passivation effect up to 0.1 mM and depassivation for higher concentrations. Generally, over the concentration domain (0.01–1.0 mM) the results reveal small inhibitive effects with maximum values of 19.7% for IO_3^- and 24–25% for MoO_4^{2-} and VO_3^- manifesting weak propensities for these inorganic species to enhance the corrosion resistance of AZ91D alloy in acidic phosphate medium. The effect of anodic potential on the characteristics of surface films formed on the alloy in alkaline phosphate solution (pH 11.9) indicates that higher forming overpotential induces better passivation due to the formation of rather thicker and more resistive anodic films. The stability of the films is greater in alkaline as compared to acidic phosphate solutions.

Keywords AZ91D alloy · Phosphate · Passivation · EIS · SEM · Potentiostatic

F. E.-T. Heakal (✉) · A. M. Fekry · M. Z. Fatayerji
Chemistry Department, Faculty of Science, Cairo University, Giza 12613, Egypt
e-mail: fakihaheakal@yahoo.com

A. M. Fekry
e-mail: hham4@hotmail.com

M. Z. Fatayerji
e-mail: mzf2001@hotmail.com

1 Introduction

Magnesium and its alloys have many unique properties compared with other metals. The most attractive feature is their low density, 1.74 g cm^{-3} for pure Mg and ca. 1.80 g cm^{-3} for most magnesium alloys, which is only one quarter of that of steel and two-thirds that of aluminum. Yet, the corrosion performance of magnesium alloys has been a major obstacle to their use in structural applications, requiring high specific strength and stiffness [1]. Development of appropriate surface treatments has led to improvement of the corrosion resistance of magnesium alloys, thus increasing their potential applications [2]. The method widely used is to generate protective layers or surface coatings by chemical conversion [3–7]. Anodizing has also been used [8]; this is usually chosen for special applications where high wear resistance or heavy-duty corrosion resistance is required.

Similarly, the addition of certain inorganic non-toxic oxysalts has a considerable effect on the corrosion performance of different metals and alloys. Among these is molybdate, successfully used to mitigate the corrosion of aluminum and aluminum alloys [9, 10], steels [11–15] and iron [16]. Likewise, in addition to its low toxicity, vanadate is used as an inhibitor of the corrosion of aluminum alloys [17, 18]. Additionally, the introduction of an oxidizing agent like KIO_3 into a corrosive acidic medium can lead to self-passivation of steel [19, 20]. Iodate has also been reported to act as an effective inhibitor for copper dissolution in acidic environments [21]. Furthermore, the above three mentioned oxyanions (MoO_4^{2-}, VO_3^- and IO_3^-) have been tested [22] as corrosion inhibitors for Ti alloy (Ti-6Al-4V) in sulphuric and hydrochloric acid solutions.

The present study aims at investigating the use of these environmentally safe anions, to enhance passivation of

magnesium-based AZ91D alloy in acidic phosphate solution (pH 4.5) using various electrochemical techniques and SEM observation. The effect of applying positive potentials on the characteristics of the surface films formed on AZ91D alloy was also examined in alkaline as well as acidic phosphate media.

2 Experimental

The working electrodes with a fixed surface area of 0.2 cm^2 were made from the as-cast AZ91D alloy as described elsewhere [23]. The alloy had a chemical composition in wt% of: 9.0 Al, 0.67 Zn, 0.33 Mn, 0.03 Cu, 0.01 Si, 0.005 Fe, 0.002 Ni, 0.0008 Be and balance Mg. The solutions were prepared using Analar grade reagents and triply distilled water. The surface of the test electrode was mechanically polished by emery papers with 400 up to 1,000 grit to ensure the same surface roughness, degreasing in acetone, rinsing with ethanol and drying in air. A typical three-electrode cell was used fitted with a large platinum sheet of size 15 × 20 × 2 mm as counter electrode and a saturated calomel (SCE) reference electrode ($E_{SCE} = 0.241$ V). Cathodic and anodic polarization curves were traced at a scan rate of 1 mV s^{-1}. Electrochemical impedance spectroscopy (EIS) were recorded with an excitation ac signal of 10 mV peak to peak in a frequency domain from 100 kHz down to 100 mHz, so that there were five measured frequency points per decade. The instrument used is a workstation IM6e (Zahner-elektrik, GmbH, Kronach, Germany).

SEM micrographs were collected using a JEOL JXA-840A electron probe microanalyzer. Potentiostatic polarization of AZ91D samples was performed in 0.1 M Na_3PO_4 solution (pH 11.8) over a potential range 0.1–3.4 V + OCP in the prepassive and passive regions. The AZ91D electrode was first immersed for 2 h in the test solution under quiescent conditions to reach steady state conditions, then potentiostating was started at the required overpotential. The electrochemical tests were carried out at 298 K.

3 Results and discussion

3.1 Chemical passivation

3.1.1 Open circuit behavior

Potential variation of the alloy was monitored over a period of 2 h in 0.1 M NaH_2PO_4 (pH 4.5) solution free of, or containing, different additions of Na_2MoO_4, $NaVO_3$ or $NaIO_3$ in the concentrations range 0.01–1.0 mM. For each solution, the potential shows a net gradual drift in the positive direction indicating continuous passivation due to healing and thickening of the naturally air formed oxide film. The spontaneous rate of potential change is high at the beginning of immersion and decreases with time reaching almost 0.0 mV min^{-1} after about 80–100 min depending on the solution composition (cf. Fig. 1a). For molybdate- and vanadate- containing solutions, an increase in concentration shifts the steady state potential (E_{st}) positively, indicating continuous film growth. However, in iodate-containing solutions critical behavior is observed, where E_{st} initially moves positively with increase in concentration up to 0.1 mM. After more addition, the potential becomes gradually more negative indicating film destruction and dissolution. The peculiar behavior of iodate addition was checked by repeating each identical test several times and repeatable data were obtained within ±4–6 mV, as shown in Fig. 1b.

According to Brasher [24], a rigid classification of anions into corrosion promoters and inhibitors was disclaimed. The author reported that corrosive or inhibitive

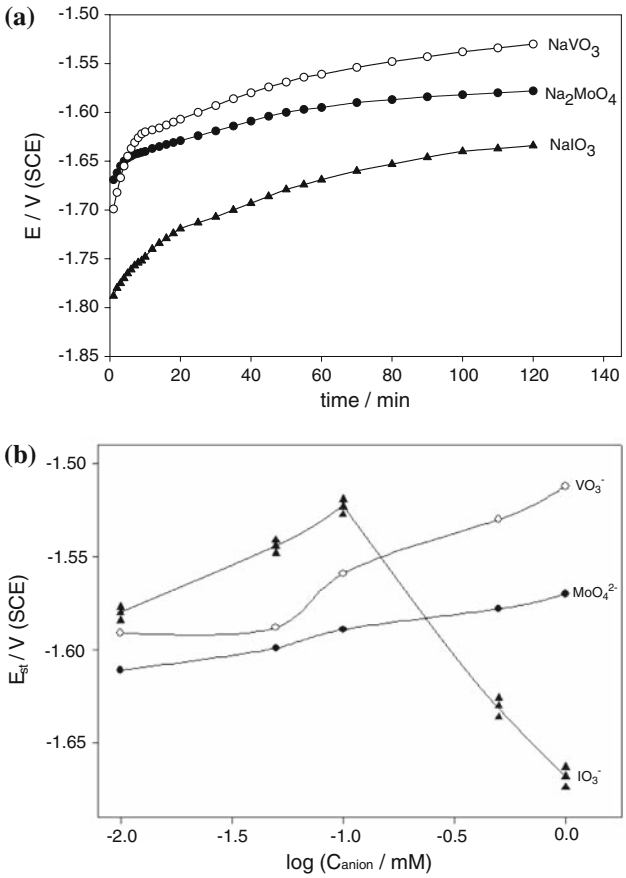

Fig. 1 **a** The OCP of AZ91D alloy as a function of time in 0.1 M NaH_2PO_4 (pH 4.5) solution containing 0.5 mM from each inhibitor. **b** Dependence of the steady state potential (E_{st}) value for AZ91D alloy on the concentration of the tested passivating anion (C_{anion}) in 0.1 M NaH_2PO_4 solution (pH 4.5), measured after 2 h immersion

properties of an electrolyte are a function of its concentration in the solution. Over the concentration range studied, Fig. 1b shows that MoO_4^{2-} and VO_3^- anions can inhibit continuously and almost linearly the corrosion of AZ91D alloy in acidic phosphate medium (pH 4.5). On the other hand, IO_3^- anion additions exhibit inhibitive properties when present in solution at large dilution (0.01–0.1 mM), and become corrosive at relatively higher concentrations (>0.1 mM), probably due to formation of soluble magnesium salt species. Furthermore, at any given concentration ≤0.1 mM, Fig. 1b shows that the quasi-steady potential of AZ91D depends on the inhibitor type, being more electropositive for IO_3^- than VO_3^- anions and more electronegative for MoO_4^{2-}, while at relatively higher additions (>0.1 mM) the sequence changes to the following order: $VO_3^- > MoO_4^{2-} > IO_3^-$.

Figure 2a, b shows EIS results probed after 2 h immersion in the molybdate-containing 0.1 M NaH_2PO_4 solution, and presented as Bode and Nyquist plots, respectively. The general features of the plots for the inhibited electrode are not substantially different from the uninhibited one. The presence of a given addition from the three tested inhibitors may increase and/or decrease both impedance and phase maximum, but does not change other aspects of the behavior. This suggests that the presence of MoO_4^{2-}, VO_3^- or IO_3^- ions in the solution do not alter the reaction responsible for corrosion, but inhibits corrosion primarily through repairing some of the defects in the naturally occurring oxide film, as well as oxidizing the active sites on the corroding surface. The Bode format (Fig. 2a) confirms the presence of two time constants as there are two maximum phase lags, regardless of the nature and concentration of the inhibitor. The first main phase lag appears at medium frequencies (MF), and the second can be seen as a shoulder at low frequencies (LF). The Nyquist format, however, is characterized by two well-defined depressed semicircles at high and medium frequency regions. Both the HF and MF capacitive loops increase with increasing added anion concentration and their dimensions depend on the inhibitor type. The spectra are dominated by the capacitance of the HF time constant.

Several trials for computer simulation of the EIS results were performed in order to establish which equivalent circuit (EC) model best fits the experimentally obtained impedance data. Figure 3 shows the proposed model consisting of two parallel combinations R_1C_1 and R_2C_2 pairs arranged in series, and in series with the solution resistance (R_s). The physical meaning of the R_1C_1 parallel circuit is likely due to the outer porous layer and the faradaic reaction therein, while R_2C_2 represents the inner barrier layer of the passive film. In parallel to R_2C_2 a resistance (R_3) in series with a Warburg impedance (Z_w) are added [25], which can be linked to ion diffusion through the passive film according

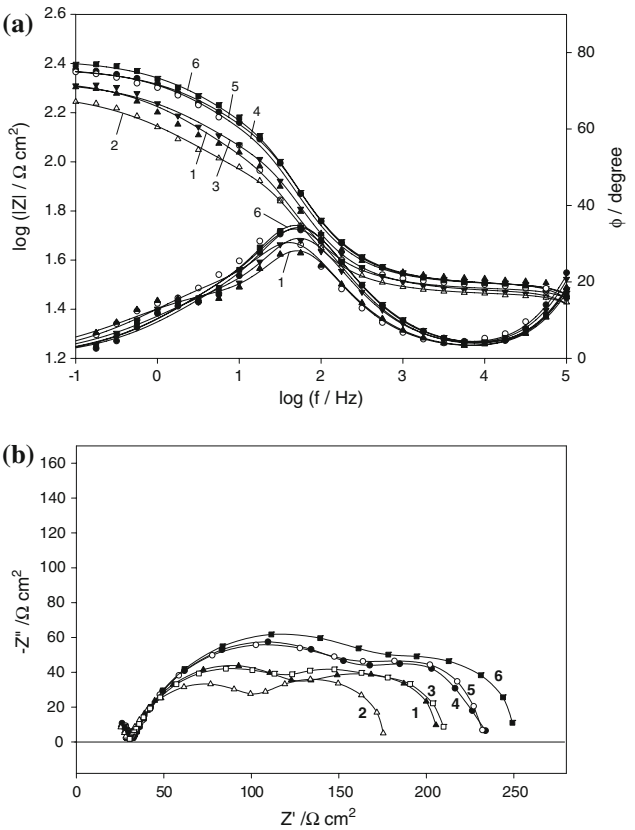

Fig. 2 EIS data of AZ91D alloy in 0.1 M NaH_2PO_4 solution (pH 4.5) after 2 h immersion, in the absence and presence of various concentrations of molybdate: (1) blank; (2) 0.01 mM; (3) 0.05 mM; (4) 0.1 mM; (5) 0.5 mM and (6) 1.0 mM. **a** The Bode plots and **b** The Nyquist plots

to the model involving electrolyte pore penetration; thereby R_3 is the electrolyte resistance in the pores. Such a diffusion process may indicate that the corrosion mechanism is controlled not only by charge-transfer but also by diffusion. In order to compensate the errors arising when using capacitance for the LF time constant (R_2C_2), a constant phase element (CPE) was considered in the EC, whose impedance takes the form: $1/C\,(j\omega)^{-1} = 1/Y^o\,(j\omega)^{-\alpha}$, where $j^2 = -1$ and α has a value between 0.5 for a porous electrode and unity for an ideal flat one [23, 26]. It can be deduced that the frequency independent constant (Y^o) of the CPE will be equal to the idealized capacitance (C) at $\omega = 1$, ω being the angular frequency ($\omega = 2\pi f$ rad s^{-1}). Very good correlation between the experimental and simulated data was found, as evident in Fig. 2a, b, where the simulated results are drawn as solid lines. The estimated values for each electrical element are listed in Table 1. The solution resistance in the pore (R_3) is always lower than R_s, due to a modification of the electrolyte conductivity by the accumulation of corrosion products in the pore. The last column of the table includes the degree of protection (P) calculated using the following relation [27]:

$$P = \left(1 - \frac{R_{T(uninh)}}{R_{T(inh)}}\right) 100 \quad (1)$$

where $R_{T(uninh)}$ and $R_{T(inh)}$ are the total resistance ($R_T = R_1 + R_2$) values of the passive film on AZ91D alloy without and with inhibitor, respectively. Table 1 shows that the presence of molybdate or vanadate in acidic phosphate solution (pH 4.5) at sufficiently great dilution ($\leq$0.01 mM) acts as corrosion promoter. However, they start to be inhibitive at relatively higher concentration. On the other hand, an opposite trend is observed for the case of iodate-containing solutions, as iodate anions inhibit the alloy corrosion at lower concentration ($\leq$0.10 mM); afterward they become corrosive. In general, the results reveal low, but satisfying, inhibitive effects, reaching maximum values of 19.9% for IO_3^- and 24.5–25.5% for MoO_4^{2-} and VO_3^-, over the concentration range studied. It is expected that the propensity of these anions to form a passive film offering better protection to AZ91D surface would be greatly improved at higher pH.

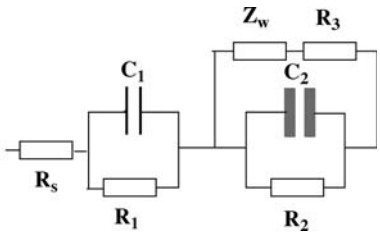

Fig. 3 The equivalent circuit model representing AZ91D alloy/electrolyte solution interface in presence of passivating anions

3.1.2 *Polarization behavior*

The anodic and cathodic (E-logi) plots shown in Fig. 4 for vanadate-containing solutions as an example, exhibit Tafel behavior which depends on the added concentration. The cathodic branch, representing the hydrogen evolution reaction (HER), shifts positively as the inhibitor concentration increases. On the other hand, over the anodic region, metal dissolution and film formation occur simultaneously; the rates are dependent on the inhibiting anionic species and its concentration. However, all anodic curves merge into a plateau due to limitations imposed by mass transfer at higher anodic potentials ($>\sim -0.7$ to -0.5 V vs. SCE).

The electrochemical corrosion parameters given in Table 2 correlate with the results derived from OCP and EIS measurements. i_{corr} in the presence of molybdate and vanadate increases a little at lower anion addition ($\leq 10^{-2}$ mM) and subsequently decreases, despite E_{corr} for both inhibitors shifting positively with increasing concentration over the whole range. The formation of soluble intermediate as a product of corrosion may facilitate the stimulation of corrosion at low concentration [24]. As the concentration increases ($>10^{-2}$ mM), this effect is overcome and inhibition increases for MoO_4^{2-} and VO_3^- anions.

A plausible mechanism for the inhibition by oxyanions involves reduction of the anions themselves. In an optimum range of concentration, depending on their nature, oxide formation and surface passivation are promoted [28]. In

Table 1 Equivalent circuit parameters for AZ91D alloy in 0.1 M NaH_2PO_4 (pH 4.5) after 2 h immersion, in the absence and presence of various concentrations from the respective passivating salt

Salt	C_{anion}/ mM	R_s/ Ω cm^2	R_1/ Ω cm^2	C_1/ μF cm^{-2}	R_2/ Ω cm^2	C_2/ μF cm^{-2}	α	R_3/ Ω cm^2	W/ kΩ cm^2 s$^{-1/2}$	R_T/ Ω cm^2	P%
Na_2MoO_4	Blank	29.6	33.2	186.4	150.3	29.6	0.79	8.5	1.53	183.5	–
	0.01	28.8	31.2	175.6	147.9	30.6	0.75	7.1	1.49	179.1	–
	0.05	29.2	39.4	172.2	160.3	26.2	0.79	8.6	1.53	199.7	8.1
	0.10	29.4	44.6	164.0	173.1	25.4	0.81	8.9	1.53	217.7	15.7
	0.50	29.3	57.2	155.5	168.5	24.4	0.81	9.0	1.54	225.7	18.7
	1.00	29.2	57.8	148.5	185.7	23.6	0.82	9.0	1.54	243.5	24.6
$NaVO_3$	0.01	29.1	31.8	174.1	146.8	31.0	0.75	6.9	1.45	178.6	–
	0.05	29.2	40.8	171.4	162.1	27.6	0.78	8.6	1.53	202.9	9.6
	0.10	29.2	44.8	165.5	174.9	25.6	0.79	8.8	1.54	219.7	16.5
	0.50	29.3	58.2	157.0	170.6	24.6	0.81	8.8	1.53	228.8	19.8
	1.00	29.1	59.0	150.1	187.4	23.8	0.81	9.0	1.55	246.4	25.5
$NaIO_3$	0.01	29.2	38.8	180.5	157.5	29.0	0.77	8.5	1.47	196.3	6.5
	0.05	29.3	47.1	178.5	168.4	28.6	0.78	8.6	1.48	215.4	14.8
	0.10	29.4	47.9	174.0	181.4	27.6	0.77	8.6	1.48	229.3	19.9
	0.50	29.5	40.4	181.5	168.0	28.5	0.78	8.6	1.48	208.4	11.9
	1.00	29.3	32.2	185.3	126.9	29.2	0.77	7.8	1.38	159.1	–

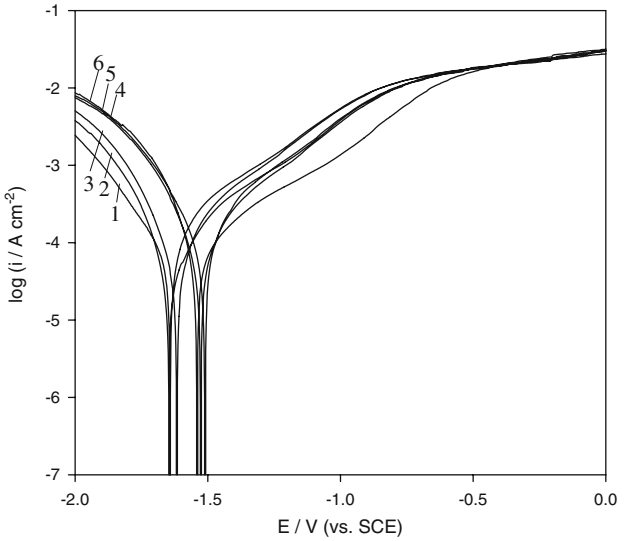

Fig. 4 Potentiodynamic cathodic and anodic polarization scans for AZ91D alloy in 0.1 M NaH_2PO_4 solution (pH 4.5) after 2 h immersion in the absence and presence of various concentrations of vanadate: (1) blank; (2) 0.01 mM; (3) 0.05 mM; (4) 0.1 mM; (5) 0.5 mM; (6) 1.0 mM

Table 2 Electrochemical corrosion parameters for AZ91D alloy in 0.1 M NaH_2PO_4 (pH 4.5) after 2 h immersion, in the absence and presence of various concentrations from the respective passivating salt

Salt	C_{anion}/ mM	i_{corr}/ μA cm^{-2}	E_{corr}/ V	P%
Na_2MoO_4	blank	92.5	−1.65	–
	0.01	97.0	−1.59	–
	0.05	85.5	−1.53	7.6
	0.10	78.5	−1.52	15.1
	0.50	75.6	−1.51	18.3
	1.00	70.3	−1.48	24.0
$NaVO_3$	0.01	94.0	−1.64	–
	0.05	91.5	−1.62	1.6
	0.10	78.2	−1.54	15.5
	0.50	72.6	−1.53	21.5
	1.00	70.0	−1.51	24.3
$NaIO_3$	0.01	86.8	−1.50	6.2
	0.05	79.4	−1.48	14.2
	0.10	74.4	−1.44	19.6
	0.50	82.2	−1.52	11.1
	1.00	95.0	−1.67	–

such cases the passive films become more stable and protect the metallic substrate from continuous corrosion. The redox reaction controls the chemistry of the film and is usually preceded by an adsorption step in which the inhibitive species adsorb on the active sites and then oxidation takes place [29]. The partial oxidizing effect of molybdate and vanadate anions enhances the oxidation of magnesium and aluminum in the corrosion sites at flawed areas via the following reactions:

For molybdate ions

$$Mg + MoO_4^- + 2H^+ = MgO + H_2O + MoO_2 \quad (2)$$

$$2Al + 3MoO_4^{2-} + 6H^+ = Al_2O_3 + 3H_2O + 3MoO_2 \quad (3)$$

For vanadate ions

$$2Mg + 2VO_3^- + 2H^+ = 2MgO + H_2O + V_2O_3 \quad (4)$$

$$4Al + 6VO_3^- + 6H^+ = 2Al_2O_3 + 3H_2O + 3V_2O_3 \quad (5)$$

In the presence of iodate anions, however, the corrosion rate of AZ91D alloy decreases at first with increase in iodate concentration reaching a minimum value at 0.1 mM, after which the rate increases. The initial decrease in corrosion rate may be for the same reason as in the presence for molybdate or vanadate anions. The adsorption of IO_3^- ions at flawed areas is the main factor for the inhibitive effect, as they facilitate the formation of aluminum and magnesium oxide according to the following redox reactions, based on the fact that solutions after all tests remained colorless:

For iodate ions

$$2Mg + IO_3^- = 2MgO + IO^- \quad (6)$$

$$2Al + IO_3^- = Al_2O_3 + I^- \quad (7)$$

On the other hand, the decrease in the inhibitive effect at iodate concentration higher than 0.1 mM may be due to iodide formation by further reduction of IO^- ions via the following equilibrium reaction:

$$IO^- + H_2O + 2e = I^- + 2OH^- \quad (8)$$

The resultant iodide ions are harmful for the magnesium alloy as they enhance the preferential dissolution of magnesium from the grain matrix and participate in the corrosion attack of the surface forming the fairly soluble magnesium iodide (MgI_2) salt [30]. Hence, the corrosion rate at these iodate levels is increased, which accords well with the experimental results.

3.1.3 SEM micrography

There is a clear color difference among the various samples, where those exposed to vanadate- or molybdate-containing solutions are darker than those exposed to iodate-containing or free-solutions. It should also be emphasized that formation of a complete surface layer of oxidation products is very difficult, and hence complete passive conditions are never achieved. This is confirmed by

SEM examination of the alloy surface after 2 h immersion in the respective inhibitor-containing 0.1 M NaH_2PO_4 solution (pH 4.5) compared to that in the free solution (the blank), as shown in Fig. 5a–d. Figure 5a shows rough platelets forming a network feature with non-uniform distribution and irregularly sized pores, defects and microcracks [31] indicating the existence of vulnerable film regions. The relatively fine β-phase ($Mg_{17}Al_{12}$) precipitated at the outer portions of the platelets has a light appearance with a shiny white color. Finally, flower-like $MnAl_2$ intermetallic inclusions [32] are also found on some areas.

Figure 5b reveals little improvement in the surface morphology of the AZ91D sample immersed in 1.0 mM iodate-containing solution, while Fig. 5c, d indicates improvement in the morphology of the films formed on the alloy exposed to 1.0 mM molybdate- or vanadate- containing solutions. These conspicuous variations in the microstructures of the films reflect the same trend of the inhibitive properties of the added salts as obtained from the electrochemical measurements.

3.2 Electrochemical passivation

The forgoing results indicate that partial passivation of AZ91D alloy is primarily dependent on the nature and morphology of the reaction product layers precipitated on its surface. In contrast to the spontaneous chemical conversion, anodizing was proved to be one of the most promising methods for producing a relative thick and uniform film with high anticorrosion performance and high adhesion to the substrate. In this part it is aimed to explore the electrochemical properties of an anodized AZ91D alloy in alkaline 0.1 M phosphate solution (pH 11.8) under controlled potential and compare its behavior with that in acidic 0.1 M phosphate solution (pH 4.5). In alkaline solution an anodic film nucleates on a corrosion film intimately contacting the substrate material [33]. To compare the behavior, measurements were conducted in the range of low overvoltage. Furthermore, to avoid possible contamination arising from chemical etching, the study was restricted to fresh mechanically polished electrodes prior to each experiment.

3.2.1 Chrono-amperometric behavior

At each applied overpotential in the range 0.1–3.4 V (vs. E_{st}), the current-time transient was monitored (i–t curve) for a period of 10 min during polarization to achieve a steady-state current value (i_{st}). Under potentiostatic conditions, the current response may be attributed to two possible processes, film formation (i_f) and film dissolution (i_d). Thus, the measured net anodic current density (i_a) is:

$$i_a = i_f + i_d \tag{9}$$

Figure 6a generally reveals that i_a drops rapidly in the first few minutes to very low values caused by fast formation and growth of an anodic passive film. i_a then becomes practically constant, indicating steady passivity. The time elapsed for the current to reach the steady state (i_{st}) value was found to increase with increasing polarization. Also, it is obvious that the passive current (i_{st}) increases with applied overpotential ($E_f - E_{st}$).

At a given polarization, the linear variation of log i_a vs. log t depicted in Fig. 6b, indicates that the anodic current density may be fitted to an empirical equation:

$$\log i_a = \text{constant} - \lambda \log t \quad (\text{where } 0 < \lambda < 1) \tag{10}$$

The absolute value of the slope, $|\lambda| = d(\log i_a)/d(\log t)$ corresponding to the passivation rate coefficient, can be taken as a measure of the degree of passivation at a given forming overpotential. The passivation tendency depends on the extent of polarization, where the estimated absolute $|\lambda|$ value is found to be higher at higher ($E_f - E_{st}$) values, as shown in Table 3. This suggests that passivity displayed by AZ91D is enhanced at higher overpotential. The exponential decay of i_a is consistent with the dependence of the electrical field strength across the film, such that the decrease in field strength, due to thickening of the anodic film, results in a decrease in i_a following the high field approximation growth law [34].

To understand the growth kinetics of the anodic passive film formed potentiostatically on AZ91D alloy, the faradaic charge density (Q) consumed during film growth at various forming overpotentials was calculated. Hence, the isochronically transported charge can be plotted against the anodizing overpotential at various transient periods during film formation, as shown in Fig. 6c. The Q – ($E_f - E_{st}$) relationship is linear and the slope increases with the forming-life period, indicating that the transported charge during polarization represents thickening of the film. The linear plots shown in Fig. 6c suggest that film thickening occurs under varying electrical field strength that is proportional to the reciprocal of the above slopes i.e. to the gradient [$d(E_f - E_{st})/dQ$] according to Faraday's law. This conclusion supports the assumption that the field in the growing anodic film decreases with increasing film thickness, in good accord with the exponential decay of the polarizing current density (Fig. 6a). At the steady state i_{st} value, however, the electrical field in the film can be considered nearly constant and the film continue growth without change in the surface charge [35].

3.2.2 Impedance behavior

Further electrochemical information concerning the anodic film stability on AZ91D alloy was also obtained by

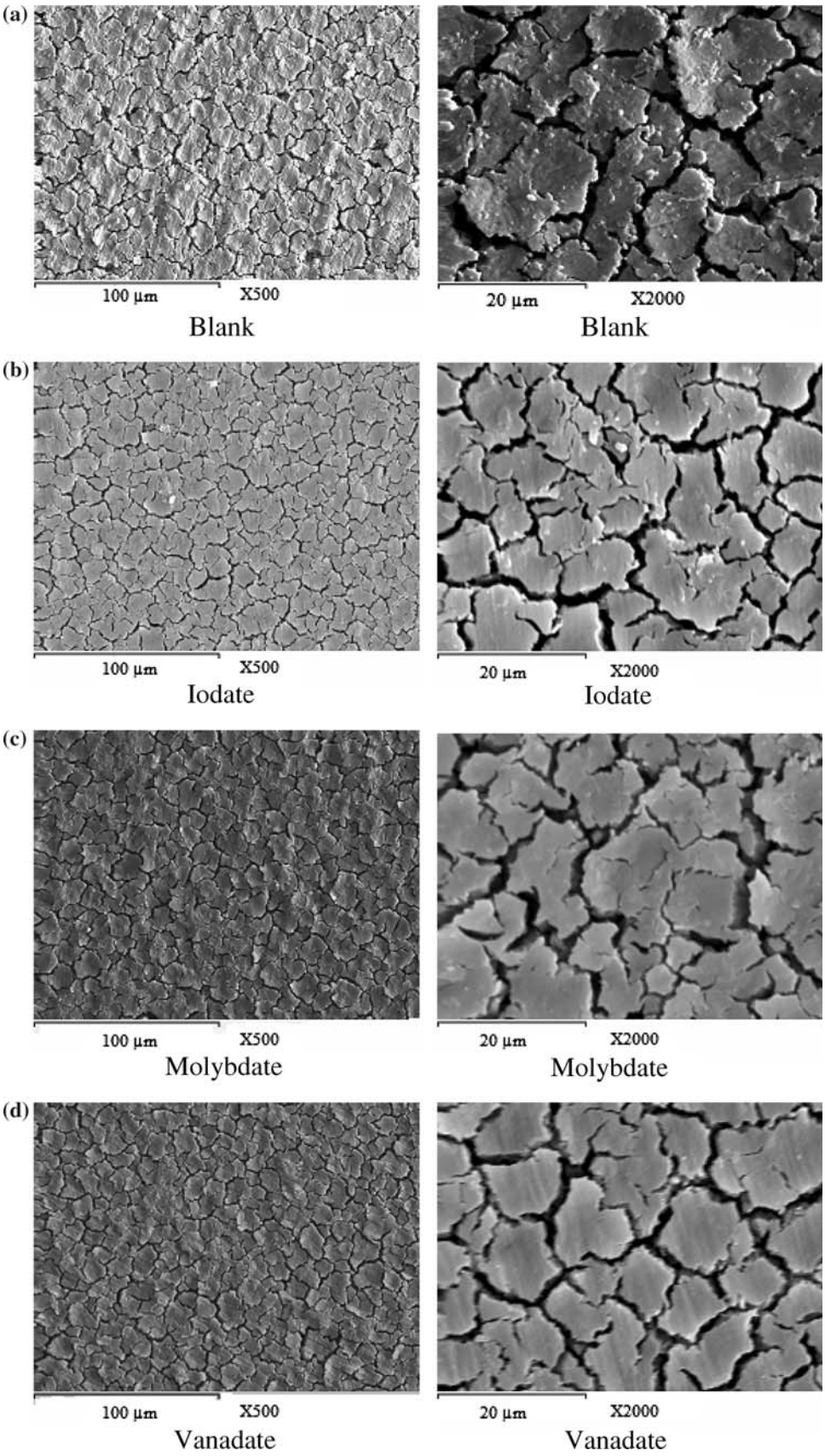

Fig. 5 **a-d** SEM morphologies at various magnifications for AZ91D surface after 2 h immersion in: **a** 0.1 M NaH_2PO_4 (blank); **b** blank + 1.0 mM $NaIO_3$; **c** blank + 1.0 mM Na_2MoO_4 and **d** blank + 1.0 mM $NaVO_3$

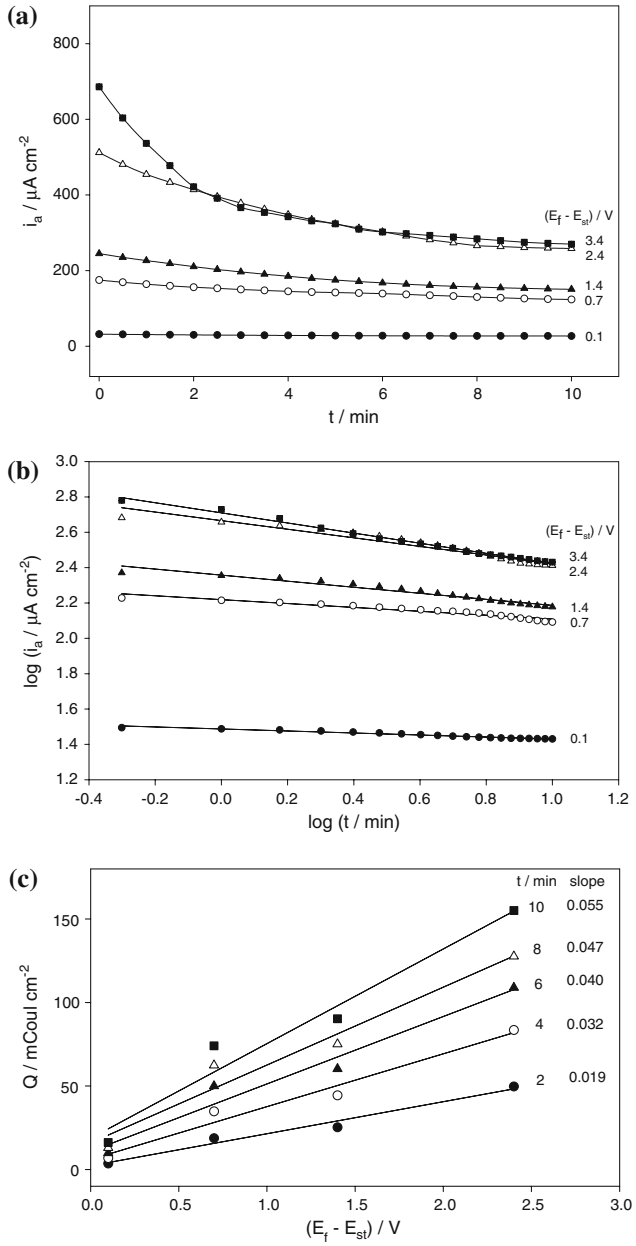

Fig. 6 **a** i-t plots for current decay during potentiostating AZ91D alloy at various anodizing overpotentials in 0.1 M Na_3PO_4 solution (pH 11.8). **b** log i-log t relationships for AZ91D alloy in 0.1 M Na_3PO_4 solution (pH 11.8), as a function of the forming overpotential ($E_f - E_{st}$). **c** Dependence of the charge density (Q) on the forming overpotential ($E_f - E_{st}$) at various anodizing periods, for AZ91D electrode in 0.1 M Na_3PO_4 (pH 11.8)

Table 3 The passivation coefficient $|\lambda|$, as a function of the forming overpotential ($E_f - E_{st}$)

($E_f - E_{st}$)/V	0.1	0.7	1.4	2.4	3.4
$\|\lambda\|$	0.06	0.11	0.17	0.24	0.29

conducting EIS in both alkaline and acidic phosphate solutions. After 10 min anodization at a specified controlled potential in 0.1 M Na_3PO_4 solution (pH 11.8), the polarization was interrupted and the impedance response of the system was directly measured in the same solution or in 0.1 M NaH_2PO_4 solution (pH 4.5). The results are presented as Bode plots in Fig. 7a, b. In both solutions the absolute impedance (|Z|) of the alloy increases with increase in forming overpotential, so that for any given value, |Z| is much higher in pH 11.9 as compared to pH 4.5, which reflects the aggressive nature of the acidic solution. This is also evident from the concomitant change in the phase maximum over the range 0.1–3.4 V where it increases from 72° to 78° in the alkaline solution, but only from 28° to 38° in the acidic one, with simultaneous shift towards higher frequencies. This behavior indicates that

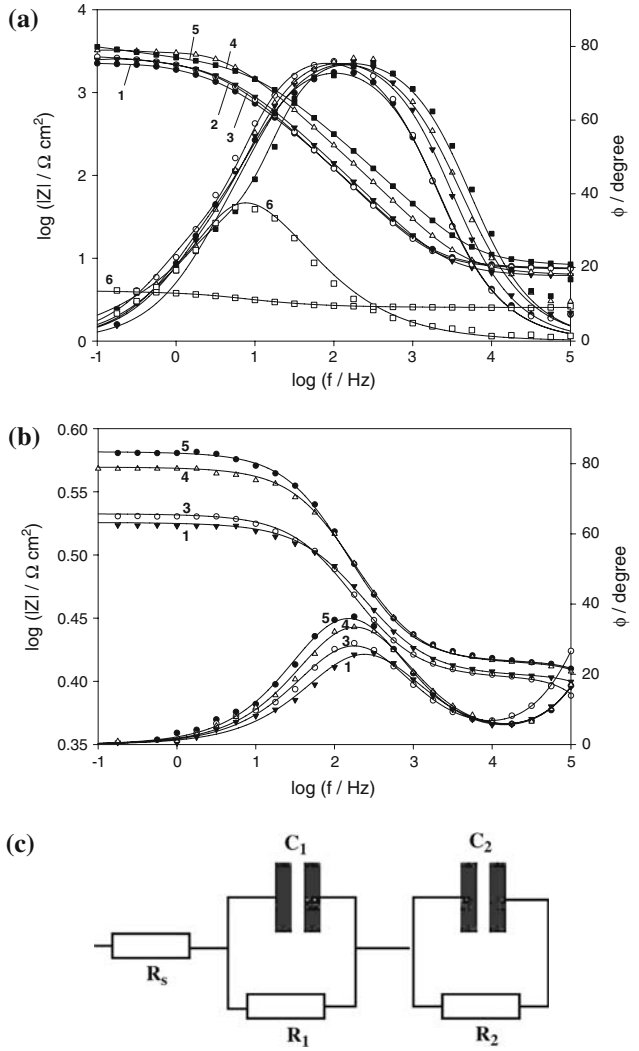

Fig. 7 The Bode plots of anodic films on AZ91D alloy formed in 0.1 M Na_3PO_4 solution (pH 11.8), at various overpotentials: (1) 0.1 V; (2) 0.7 V; (3) 1.4 V; (4) 2.4 V; (5) 3.4 V. The behavior in: **a** 0.1 M Na_3PO_4 (pH 11.8) and **b** 0.1 M NaH_2PO_4 (pH 4.5). (6) The behavior in 0.1 M NaH_2PO_4 (pH 4.5) for the film formed at 3.4 V in the same acidic phosphate solution. **c** The equivalent circuit model representing AZ91D alloy/anodic film/solution system

Table 4 Equivalent circuit parameters of the anodic films on AZ91D alloy immersed in 0.1 M Na_3PO_4 solution (pH 11.8) as a function of the anodic forming overpotential ($E_f - E_{st}$). The behavior in: (a) 0.1 M Na_3PO_4 (pH 11.8) and (b) 0.1 M NaH_2PO_4 (pH 4.5)

$E_f - E_{st}$/ V	R_s/ Ω cm^2	R_1/ kΩ cm^2	C_1/ μF cm^{-2}	α_1	R_2/ Ω cm^2	C_2/ μF cm^{-2}	α_2	R_T/ kΩ cm^2	$1/C_T$/ μF^{-1} cm^2
(*a*)									
0.1	7.6	1.67	20.34	0.84	671	24.4	0.93	2.34	0.09
0.7	7.3	1.89	19.12	0.81	771	21.2	0.99	2.66	0.10
1.4	6.9	2.15	13.42	0.83	821	19.8	0.97	2.97	0.13
2.4	7.0	2.58	9.08	0.86	854	16.3	0.95	3.43	0.17
3.4	7.8	2.65	8.97	0.78	906	13.8	0.99	3.56	0.19
3.4[a]	5.3	0.17	68.5	0.60	51.9	88.9	0.98	0.24	0.03
(*b*)									
0.1	1.18	0.06	21.3	0.74	19.6	28.2	0.61	0.08	0.08
1.4	1.19	0.07	18.1	0.74	19.8	27.9	0.64	0.09	0.09
2.4	1.35	0.12	12.7	0.75	22.0	26.9	0.66	0.14	0.12
3.4	1.37	0.14	11.6	0.75	22.3	26.6	0.67	0.16	0.13

[a] Parameters for the film formed at 3.4 V in 0.1 M NaH_2PO_4 solution and measured in the same solution (pH 4.5)

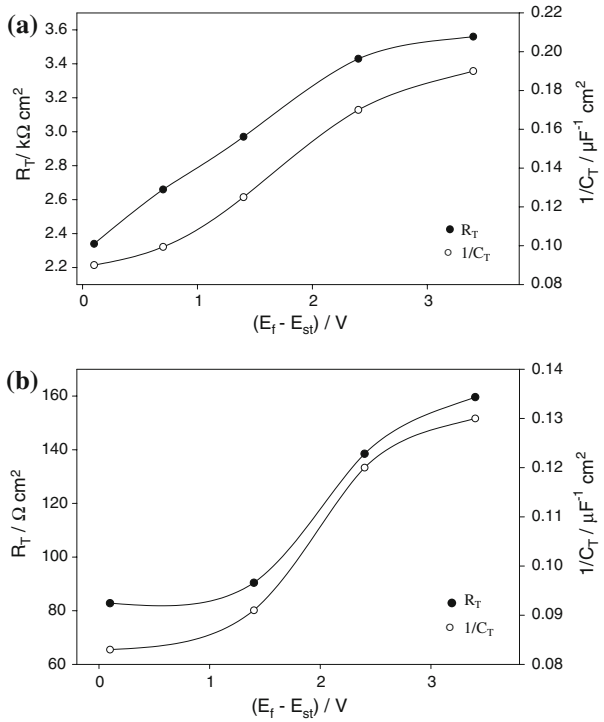

Fig. 8 The total resistance (R_T) and relative thickness ($1/C_T$) of the anodic films formed on AZ91D alloy in 0.1 M Na_3PO_4 solution (pH 11.8) as a function of the anodic forming overpotential ($E_f - E_{st}$). The behavior in: **a** 0.1 M Na_3PO_4 (pH 11.8) and **b** 0.1 M NaH_2PO_4 (pH 4.5)

higher forming overpotentials and/or pH of the medium significantly improved the protective performance of the passive film and cause noticeable increase in its stability. Figure 7a also includes the Bode plot (curve 6) for the film formed at 3.4 V in acidic phosphate and measured in the same solution. This test clearly shows that acidic medium is not suitable to form or maintain a passive film on AZ91D as magnesium is unstable at lower pH (<11.0) [36].

The experimental impedance plots were analyzed using a suitable EC model comprising series R_1C_1 and R_2C_2 parallel combinations in series with the solution resistance (R_s) as given in Fig. 7c. This clearly shows that the anodic films have bilayered structure, where the HF time constant (R_1C_1) originates from the outer layer and the LF one (R_2C_2) is assigned to the inner layer of the film [37]. For this model the electrode impedance is represented by the following transfer function [30, 38, 39]:

$$Z(w) = R_s + \frac{R_1}{1 + (j\omega)^{\alpha_1} C_1 R_1} + \frac{R_2}{1 + (j\omega)^{\alpha_2} C_2 R_2} \qquad (11)$$

The above formula takes into account the deviation from the ideal RC behavior and considers, for a more realistic approach, that each oxide layer as non-homogeneous. Thereby, the impedance associated with the capacitance of each layer is described by a CPE [40]. The calculated equivalent circuit parameters given in Table 4a, b show clearly that the increase in overpotential generally increases the two resistance values R_1 and R_2 corresponding to the outer and inner layers of the anodic passive film, respectively, while their associated capacitance values C_1 and C_2 decrease. This behavior suggests that high potential is essential for forming a good anodic film with excellent insulating properties which exhibits better stability at higher pH. The outer layer of the passive film incorporates PO_4^{3-} species from the electrolyte in its structure during anodizing, hence, higher R_1 values were recorded for this layer compared to R_2 for the inner one [23].

It can be seen from Fig. 8a, b that the total passive film resistance (R_T) increases with the forming overpotential, giving a sigmoidal-shaped curve in both alkaline and acidic

phosphate solutions. The passive film thickness (d) is directly proportional to the reciprocal total capacitance of the passive film ($1/C_T = 1/C_1 + 1/C_2$) [8, 39] in accordance to the relation: $1/C_T = d/\varepsilon_o\varepsilon_r A$, where A is the film area, ε_o and ε_r are the dielectric constants of vacuum and film, respectively. Figure 8a, b shows that the trends of the passive film thickness ($1/C_T$) in alkaline and acidic solutions are mirrored completely by those of their corresponding R_T values. Thus the increase in total passive film resistance is mainly attributable to thickening process of the oxide film at higher anodic potential. This behavior is in good agreement with the trend for the steady state current (i_{st}), and indicates generally that higher anodizing overpotentials (>2.4 V) facilitate the dissolution process such that the film dissolution rate becomes comparable with its formation rate, hence a steady state film thickness and resistance are achieved. The results are consistent with film growth via a dissolution-precipitation mechanism [41].

4 Conclusions

1. Molybdate and vanadate anions additions in excess of 10^{-2} mM can induce passivation of AZ91D in acidic phosphate solution (pH 4.5), with an efficiency of 24.5–25.5% at 1.0 mM. However, iodate anion exhibits critical behavior with a maximum passivation effect of 19.9% at 0.1 mM addition.
2. Applying a controlled anodic potential (0.1–3.4 V, vs. OCP) can also induce passivation of different degrees to AZ91D in alkaline phosphate solution (pH 11.8).
3. The passive film resistance was found to increase with increasing overpotential, mainly due to film thickening at higher positive potential.
4. The results reveal that the chemical conversion approach can improve the passive behavior of AZ91D alloy in acidic phosphate solution. An additional improvement is expected at higher pH. On the other hand, the anodic film approach is valid in alkaline conditions, as the film stability is found to be much reduced at lower pH.

References

1. Ghali E (2000) Magnesium and magnesium alloy. In: Revie RW (ed) Uhlig corrosion handbook. Wiley, New York
2. Eliezer D, Aghion E, Froes FH (1998) Adv Perform Mater 5:201
3. Avedesin M (1999) In: Baker H (ed) Magnesium and magnesium alloys, ASM specialty handbook. ASM International, Materials Park, OH
4. Huo H, Li Y, Wang F (2004) Corros Sci 46:467
5. Reiners G, Griepentrog M (1995) Surf Coat Technol 76–77:809
6. Rudd AL, Breslin CB, Mansfeld F (2000) Corros Sci 42:275
7. Zozulin AJ, Bartak DE (1994) Met Finish 92:39
8. Zhang LJ, Fan JJ, Zhang Z, Cao FH, Zhang JQ, Cao CN (2007) Electrochim Acta 52:5325
9. Emregül KC, Aksüt AA (2003) Corros Sci 45:2415
10. Breslin CB, Treacy G, Carroll WM (1994) Corros Sci 36:1143
11. Mu G, Li X, Qu Q, Zhou J (2006) Corros Sci 48:445
12. Zhao JM, Zuo Y (2002) Corros Sci 44:2119
13. Lemaitre C, Baroux B, Beranger G (1990) Corros Sci 31:585
14. Alentejano CR, Aoki IV (2004) Electrochim Acta 49:2779
15. Saremi M, Dehghanian C, Sabet MM (2006) Corros Sci 48:1404
16. Virtanen S, Surber B, Nylund P (2001) Corros Sci 43:1165
17. Iannuzzi M, Kovacb J, Frankel GS (2007) Electrochim Acta 52:4032
18. Iannuzzi M, Frankel GS (2007) Corros Sci 49:2371
19. Shibli SMA, Saji VS (2005) Corros Sci 47:2213
20. Sato E, Honma K (2001) Japanese Patent JP 81:573
21. Luo Q (2000) Langmuir 16:5154
22. Mogoda AS, Ahmad YH, Badawy WA (2004) Mat Corros 55:449
23. El-Taib Heakal F, Fekry AM, Fatayerji MZ (2008) J Appl Electrochem (in press)
24. Brasher DM (1962) Nature 183:868
25. Beccaria AM, Bertolotto C (1997) Electrochim Acta 42:1361
26. Rammelt U, Reinhard G (1990) Electrochim Acta 35:1045
27. Szklarska-Smialowska Z (1991) Electrochemical and optical techniques for the study of metallic corrosion. Kluwer Academic Publishers, Dordrecht, p 545
28. Brett CMA, Gomes IAR, Martins JPS (1994) J Appl Electrochem 24:1158
29. Zein El-Abedin S (2001) J Appl Electrochem 31:711
30. El-Taib Heakal F, Fekry AM, Fatayerji MZ (2009) Electrochim Acta 54:1545
31. Zhou W, Shan D, Han E-H, Ke W (2008) Corros Sci 50:329
32. Pardo A, Merino MC, Coy AE, Arrabal R, Viejo F, Matykina E (2008) Corros Sci 50:823
33. Birss VI, Xia S, Yue R, Rateick RG Jr (2004) J Electrochem Soc 151:B1
34. Güntherschulz A, Betz H (1934) Z Phys 92:367
35. Hurlen T, Hornkiol S (1991) Electrochim Acta 36:189
36. Pourbaix M (1974) Atlas of electrochemical equilibria in aqueous solutions. NACE, Houston, p 136
37. Mansfeld F, Kendig MW (1988) J Electrochem Soc 135:828
38. Patrito EM, Macagno VA (1994) J Electroanal Chem 375:203
39. El-Taib Heakal F, Fekry AM, Ghoneim AA (2008) Corros Sci 50:1618
40. Jüntter K (1990) Electrochim Acta 35:1501
41. Armstrong RD (1971) Corros Sci 11:693